

# Averaged Modeling of PWM Converters Operating in Discontinuous Conduction Mode

Jian Sun, *Member, IEEE*, Daniel M. Mitchell, *Senior Member, IEEE*, Matthew F. Greuel, Philip T. Krein, *Fellow, IEEE*, and Richard M. Bass, *Senior Member, IEEE*

**Abstract**—Various aspects of averaged modeling of hard-switching pulse-width modulated (PWM) converters operating in the discontinuous conduction mode (DCM) are studied. A more streamlined modeling procedure is proposed which serves as a general framework for comparing different models. A duty ratio constraint that defines the diode conduction interval is identified to be the key to accurate prediction of high-frequency behavior. A new duty-ratio constraint is proposed that leads to full-order averaged models of DCM converters. Numerical analyses and experimental measurements confirm that the new models correctly predict the small-signal responses up to one third of the switching frequency and are more accurate than all previous models. Moreover, new analytical results are included to show the origin of the high-frequency pole in DCM operation and to explain why the full-order model is capable of accurately predicting it. Averaged circuit counterparts of the new models are developed in the form of averaged switch models to facilitate circuit simulation.

**Index Terms**—Averaged modeling, averaged switch model, discontinuous conduction mode, PWM converters.

## I. INTRODUCTION

THE discontinuous conduction mode (DCM) of operation typically occurs in dc/dc converters at light load. For low-power applications, many designers prefer to operate the converter in DCM even at full load in order to avoid the reverse recovery problem of the diode. DCM operation has also been considered a possible solution to the right-half plane (RHP) zero problem encountered in buck-boost and boost derived topologies. In single-phase ac/dc converters with active power factor correction (PFC), the input inductor current becomes discontinuous in the vicinity of the voltage zero crossing; some PFC circuits are even purposely designed to operate in DCM over the entire line cycle in order to simplify the control [1], [2]. Proper analytical models for DCM operation of PWM converters are therefore essential for the analysis and design of converters in a variety of applications.

Many efforts have been made in the past two decades to model DCM PWM converters [3]–[6]. These models are given either

in analytical form [3], [5] or as equivalent circuits [4], [6], and fall into two categories:

- 1) reduced-order models [3], [4];
- 2) full-order models [5], [6].

In reduced-order models, the inductor current (or one of the inductor currents when there are multiple inductors) does not appear as a state variable. A reduced-order model can correctly predict the behavior of a converter in the low-frequency range. However, large discrepancies appear at high frequencies (above about one-tenth of the switching frequency), particularly in the phase response. Also, the absence of the inductor current in the averaged model is undesirable for applications such as single-phase PFC in which the inductor current is the ultimate control target.

More recently, full-order averaged models have been reported for DCM PWM converters [5], [6]. Although developed independently and presented in different forms, the analytical model presented in [5] and the averaged circuit model in [6] can be shown to be equivalent. The inductor current is retained in these full-order averaged models, and they have shown improved accuracy over reduced-order models. However, relatively large discrepancies still exist at high frequencies, as will be shown later in this paper. Moreover, the model developments in [5], [6] did not include analysis of accuracy, and it was not quite clear what attributes of these full-order models contribute to their improved accuracy.

Considering the unsatisfactory situation in the modeling of discontinuous conduction mode, an effort was undertaken by the authors to study the various issues involved, started with a reexamination of all existing models. The current paper is a compilation of the major results evolved from that effort. To be specific, we will present a physically-based modeling procedure for PWM converters which serves as a general framework for comparing different models, along with new full-order averaged models, in both analytical and circuit forms, that overcome the hitherto mentioned problems of existing models.

The paper is organized as follows: The next section reexamines the conventional state-space averaging method for DCM PWM converters [3] by streamlining the procedures. An alternative approach to deriving reduced-order averaged models will be presented. Section III introduces the concept of a duty-ratio constraint, which defines the diode conduction interval and leads to new, full-order averaged models. The new models are compared with existing models in Section III, and then verified in Section IV by numerical simulation and experimental measurements. Section V provides more analytical results to show the

Manuscript received March 27, 2000; revised March 16, 2001. Recommended by Associate Editor C. K. Tse.

J. Sun and D. M. Mitchell are with the Advanced Technology Center, Rockwell Collins, Inc., Cedar Rapids, IA 52498 USA (e-mail: jsun@collins.rockwell.com).

M. F. Greuel is with R. R. Donnelley and Sons, Mattoon, IL 61938 USA.

P. T. Krein is with the Department of Electrical and Computer Engineering, University of Illinois, Urbana, IL 61801 USA.

R. M. Bass, deceased, was with the School of Electrical and Computer Engineering, Georgia Institute of Technology, Atlanta, GA 30332 USA.

Publisher Item Identifier S 0885-8993(01)05958-0.

origin of the high-frequency pole in DCM operation and to explain why the new models are capable of correctly predicting the high-frequency pole. Section VI presents an averaged switch model that can be used to replace the PWM switch cell. This results in a circuit model that is equivalent to the new analytical model. Section VII offers conclusions.

## II. GENERAL FRAMEWORK

The DCM operation of PWM converters differs from CCM (continuous conduction mode) operation by an additional time interval in each switching cycle during which an inductor current or capacitor voltage is clamped to zero (or a constant when there are multiple energy storage elements). Consider a dc-dc converter with two switches (or two equivalent switches, in the case of bridge-type forward converters). For DCM operation involving inductors, the inductor current rises in the first interval when the switch is turned on, reaches a peak when the switch is to be turned off, and resets to zero (or a constant) at the end of the second interval. In the discussions hereafter, we use  $d_1$  and  $d_2$  to denote the duty ratio of the first and the second interval, respectively (see Fig. 1). Assume also that the converter power stage can be described accurately with a piecewise-linear state-space model. Let  $v_{in}$  denote the input voltage of the converter while  $T_s$  denotes the length of a switching cycle. Then

$$\dot{\mathbf{x}} = \mathbf{A}_1 \mathbf{x} + \mathbf{b}_1 v_{in} \quad \text{for } t \in [0, d_1 T_s] \quad (1)$$

$$\dot{\mathbf{x}} = \mathbf{A}_2 \mathbf{x} + \mathbf{b}_2 v_{in} \quad \text{for } t \in [d_1 T_s, (d_1 + d_2) T_s] \quad (2)$$

$$\dot{\mathbf{x}} = \mathbf{A}_3 \mathbf{x} + \mathbf{b}_3 v_{in} \quad \text{for } t \in [(d_1 + d_2) T_s, T_s]. \quad (3)$$

Notice that the second duty ratio,  $d_2$ , in DCM is not independent, but rather has algebraic dependency on state and control variables. For the purposes of an averaged model, it is necessary to reflect this dependency in terms of the average values of voltage and current. That way,  $d_2$  can be eliminated, and a model expressed solely in the averaged state variables can be obtained. The algebraic function defining this dependency is called the *duty-ratio constraint* in this paper.

The modeling method we employ for DCM operation consists of three steps:

- 1) averaging;
- 2) inductor current analysis;
- 3) duty-ratio constraint.

The first two steps are discussed in the following subsection, while the third step will be detailed in Section II-B and Section III.

### A. Averaging and Correction

As in the continuous conduction mode, state-space averaging can be applied to (1)–(3) to give the following averaged model:

$$\begin{aligned} \dot{\bar{\mathbf{x}}} = & [d_1 \mathbf{A}_1 + d_2 \mathbf{A}_2 + (1 - d_1 - d_2) \mathbf{A}_3] \bar{\mathbf{x}} \\ & + [d_1 \mathbf{b}_1 + d_2 \mathbf{b}_2 + (1 - d_1 - d_2) \mathbf{b}_3] v_{in}. \end{aligned} \quad (4)$$

As usual, we use  $\bar{\mathbf{x}}$  to denote the average of  $\mathbf{x}$  over an entire switching cycle.

The problem with the state-space averaging approach in DCM is that we are averaging just the matrix parameters, and

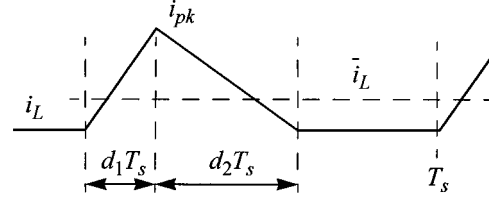


Fig. 1. Inductor current waveform of PWM converter in DCM.

TABLE I  
CHARGING OF CAPACITOR BY AN INDUCTOR OPERATING IN DCM

Inductor Charging Capacitor	SSA Equivalent Charging Current	Actual Equivalent Charging Current
When Switch is On	$i_L d_1 = \frac{i_{pk} d_1}{2} \cdot (d_1 + d_2)$	$\frac{i_{pk} d_1}{2}$
When Switch is Off	$i_L d_2 = \frac{i_{pk} d_2}{2} \cdot (d_1 + d_2)$	$\frac{i_{pk} d_2}{2}$
Over the Entire Cycle	$i_L (d_1 + d_2) = \frac{i_{pk}}{2} \cdot (d_1 + d_2)^2$	$\frac{i_{pk}}{2} \cdot (d_1 + d_2)$

not necessarily the state variables themselves. It is intended that (4) will apply when the true average of each state variable is used, but the average inductor current depends on the parameters and duty ratios. Consider instead a formal averaging approach [7], in which the sets of equations are written out in terms of switching functions  $d_1$  and  $d_2$ . The principle is to write out the complete Kirchhoff's Laws expressions for each energy storage device, and perform the averaging step only on the final equations. In a two-state power converter, this entails writing expression for the inductor and the KCL expression for the capacitor, then averaging over the switching interval. The DCM interval is given by  $1 - d_1 - d_2$ . When the average is to be taken, product terms like  $[d_1 a_1 + d_2 a_2 + (1 - d_1 - d_2) a_3] i_L$  will result, where  $a_1$ ,  $a_2$ , and  $a_3$  are topology-dependent coefficients. In CCM, the average of the products  $d i_L$  is the same as the product of the averages, and state-space averaging gives the same result as formal averaging of the circuit equations. In contrast, in DCM the average of product terms  $d i_L$  will not be the same as the product of the averages.

Based on the waveform shown in Fig. 1, this average can be written as

$$\bar{i}_L = \frac{i_{pk}}{2} \cdot (d_1 + d_2). \quad (5)$$

The KVL expression for the inductor is essentially the same as in continuous mode, except that a new unknown,  $d_2$ , appears. Now consider a general case in which a capacitor is connected to the inductor when the switch is on ( $t \in [0, d_1 T_s]$ ). The current delivered to the capacitor is not necessarily the same as the average inductor current. Since the inductor current is changing rapidly with time, it is convenient to formulate the capacitor equation in terms of conservation of charge, then perform the averaging step. In this case the total amount of charge the capacitor receives from the inductor over a switching cycle is

$$Q_c = \frac{i_{pk} d_1 T_s}{2}$$

which is equivalent to an average charging current of

$$\frac{Q_c}{T_s} = \frac{i_{pk}d_1}{2}. \quad (6)$$

If the capacitor is connected to a resistive load, the net charge delivered to the capacitor is  $(i_{pk}d_1)/2 - v_C/R$ . On the average

$$C \frac{dv_C}{dt} = \frac{i_{pk}d_1}{2} - \frac{v_C}{R}.$$

This result is a fundamental implication of charge conservation in the capacitor. Notice, however, that it is not the same as the KCL expression for the capacitor generated by state-space averaging. The state-space averaged model (4) would imply that the equivalent average current charging the capacitor is  $\bar{i}_L d_1$ , that is, the average of the inductor current times the duty ratio of the subinterval in which the capacitor is charged by the inductor, which will be called the state-space-averaged (SSA) charging current. Using (5), the SSA equivalent charging current can be written as

$$\bar{i}_L d_1 = \frac{i_{pk}d_1}{2} \cdot (d_1 + d_2) \quad (7)$$

which is different from the actual charging current identified in (6). The implication is that an unmodified SSA approach, in which the averaging step is performed on a complete model rather than on the equations themselves, might not preserve charge conservation under DCM conditions. The correction to reflect (6) does not involve any inconsistency: In continuous mode, the conventional SSA model results regardless of how the averaging step is performed. In DCM, the rapid change in inductor current requires that averaging be performed more formally on the KVL and KCL expressions.

Table I shows the difference between the actual average charging current and the SSA charging current for a capacitor that is connected to the inductor when the switch is on, off, or over the entire switching cycle. Responses defined by the original state-space averaged model (4) would be expected not to match the actual averaged response of the converter because of these differences. A modification of (4) is therefore necessary to correct for this mismatch. As can be seen from Table I, this can be achieved by dividing inductor current(s) on the right-hand side of (4) by the factor  $d_1 + d_2$ . A systematic approach to this is to rearrange the state vector  $\mathbf{x}$  such that  $\mathbf{x} = [\mathbf{i}_L \ v_C]^T$ , where subvector  $\mathbf{i}_L$  contains all ( $n_L$ ) inductor currents of the converter, and define a matrix  $\mathbf{M}$  as follows:

$$\mathbf{M} = \text{diag} \left[ \underbrace{\frac{1}{d_1 + d_2}, \dots, \frac{1}{d_1 + d_2}}_{n_L}, 1, \dots, 1 \right]. \quad (8)$$

With this, the modified averaged model that would correctly predict the behavior in DCM becomes

$$\begin{aligned} \dot{\hat{\mathbf{x}}} = & [d_1 \mathbf{A}_1 + d_2 \mathbf{A}_2 + (1 - d_1 - d_2) \mathbf{A}_3] \mathbf{M} \hat{\mathbf{x}} \\ & + [d_1 \mathbf{b}_1 + d_2 \mathbf{b}_2 + (1 - d_1 - d_2) \mathbf{b}_3] v_{in}. \end{aligned} \quad (9)$$

### B. Example—Boost Converter

As an example, we consider the boost converter depicted in Fig. 3. With  $\mathbf{x} = [i_L \ v_C]^T$  chosen as the state vector, the state matrices and input vectors of the converter are

$$\begin{aligned} \mathbf{A}_1 &= \begin{bmatrix} 0 & 0 \\ 0 & -\frac{1}{RC} \end{bmatrix}, \quad \mathbf{A}_2 = \begin{bmatrix} 0 & -\frac{1}{L} \\ \frac{1}{C} & -\frac{1}{RC} \end{bmatrix}, \quad \mathbf{A}_3 = \begin{bmatrix} 0 & 0 \\ 0 & -\frac{1}{RC} \end{bmatrix}, \\ \mathbf{b}_1 &= \begin{bmatrix} \frac{1}{L} \\ 0 \end{bmatrix}, \quad \mathbf{b}_2 = \begin{bmatrix} \frac{1}{L} \\ 0 \end{bmatrix}, \quad \mathbf{b}_3 = \begin{bmatrix} 0 \\ 0 \end{bmatrix}. \end{aligned}$$

The state-space averaged model of the converter corresponding to (4) is

$$\frac{d}{dt} \begin{bmatrix} \bar{i}_L \\ \bar{v}_C \end{bmatrix} = \begin{bmatrix} 0 & -\frac{d_2}{L} \\ \frac{d_2}{C} & -\frac{1}{RC} \end{bmatrix} \begin{bmatrix} \bar{i}_L \\ \bar{v}_C \end{bmatrix} + \begin{bmatrix} \frac{d_1 + d_2}{L} \\ 0 \end{bmatrix} v_{in}.$$

Since there is only one inductor and the dimension of  $\mathbf{x}$  is two, the modification matrix  $\mathbf{M}$  is simply

$$\mathbf{M} = \begin{bmatrix} \frac{1}{d_1 + d_2} & 0 \\ 0 & 1 \end{bmatrix}.$$

Hence the modified averaged model of this boost converter in DCM is

$$\begin{aligned} \frac{d}{dt} \begin{bmatrix} \bar{i}_L \\ \bar{v}_C \end{bmatrix} &= \begin{bmatrix} 0 & -\frac{d_2}{L} \\ \frac{d_2}{C} & -\frac{1}{RC} \end{bmatrix} \mathbf{M} \begin{bmatrix} \bar{i}_L \\ \bar{v}_C \end{bmatrix} + \begin{bmatrix} \frac{d_1 + d_2}{L} \\ 0 \end{bmatrix} v_{in} \\ &= \begin{bmatrix} 0 & -\frac{d_2}{L} \\ \frac{d_2}{C(d_1 + d_2)} & -\frac{1}{RC} \end{bmatrix} \begin{bmatrix} \bar{i}_L \\ \bar{v}_C \end{bmatrix} + \begin{bmatrix} \frac{d_1 + d_2}{L} \\ 0 \end{bmatrix} v_{in}. \end{aligned} \quad (10)$$

### C. Reduced-Order Averaged Models

As previously pointed out, a duty-ratio constraint defining the dependency of  $d_2$  on other variables is needed to complete the averaged model (9). In the conventional state-space averaging method [3], a volt-second balance relation of the inductor is used to define the duty-ratio constraint. For the boost topology, volt-second balance over a switching cycle implies

$$d_2 = \frac{v_{in}}{\bar{v}_C - v_{in}} \cdot d_1. \quad (11)$$

Substituting this into (10) yields the following equations:

$$\frac{d\bar{i}_L}{dt} = 0, \quad (12)$$

$$\frac{d\bar{v}_C}{dt} = \frac{v_{in}}{\bar{v}_C} \cdot \frac{\bar{i}_L}{C} - \frac{\bar{v}_C}{RC}. \quad (13)$$

This is a degenerate model where the dynamics of the inductor current disappear. In fact, it can be readily verified that use of the volt-second balance relation will always result in a degenerate model. Since the inductor current is no longer a state variable in this averaged model, it must be expressed as an algebraic function of other variables, resulting in a reduced-order averaged model that is independent of inductor dynamics.

For the boost converter, since the peak of the inductor current is

$$i_{pk} = \frac{v_{in}}{L} \cdot d_1 T_s \quad (14)$$

the average of the inductor current can be written as

$$\bar{i}_L = \frac{i_{pk}}{2} \cdot (d_1 + d_2) = \frac{v_{in}}{2L} \cdot d_1(d_1 + d_2)T_s.$$

With (11), the above relation can be simplified to

$$\bar{i}_L = \frac{i_{pk}}{2} \cdot (d_1 + d_2) = \frac{v_{in}}{2L} \cdot \frac{d_1^2 T_s \bar{v}_C}{\bar{v}_C - v_{in}}$$

which can now be substituted into (13) to eliminate its dependency on  $\bar{i}_L$ . The result is the conventional reduced-order averaged model for boost converter in DCM [3], as given below

$$\frac{d\bar{v}_C}{dt} = \frac{v_{in}^2}{2LC} \cdot \frac{d_1^2 T_s}{\bar{v}_C - v_{in}} - \frac{\bar{v}_C}{RC}. \quad (15)$$

#### D. A New Approach to Reduced-Order Modeling

The absence of the inductor current in the conventional reduced-order averaged model is the result of an implicit assumption that the dynamics of inductor current become so fast in DCM that they can be neglected at low frequencies. The conventional approach as outlined before does not make this assumption explicitly, which has caused some confusion. On the other hand, if this assumption is made explicitly beforehand, the reduced-order averaged model can be derived in a more streamlined way. In general, the problem then becomes as follows. Given a system that has both fast and slowly changing variables, how should one derive a (reduced-order) averaged model that represents the slow dynamics of the system? A general method, first presented in the converter averaging context in [8], can be applied for this purpose. The method consists of three steps, outlined as follows (see [9]).

- 1) Calculate the response of the fast variables over a switching cycle. The slow variables are assumed to be constant during this calculation.
- 2) Substitute for the fast variables in slow variable models with the responses calculated in step 1). This eliminates the dependence of slow variable models on the fast variables.
- 3) Average the resulting *decoupled* slow variable models over a switching cycle. The result is a reduced-order averaged model for the slow variables.

We use again the boost converter as example to demonstrate the application of this method. Referring to Fig. 3 and assuming that  $v_C$  is constant, the response of the inductor current over a switching cycle can be calculated as follows:

$$i_L = \frac{1}{L} \begin{cases} v_{in} \cdot t & t \in [0, d_1 T_s] \\ v_{in} d_1 T_s - (v_C - v_{in})t & t \in [d_1 T_s, (d_1 + d_2) T_s] \\ 0 & t \in [(d_1 + d_2) T_s, T_s] \end{cases} \quad (16)$$

In addition,  $d_2$  can be determined as follows from the fact that  $i_L$  resets to zero at  $t = (d_1 + d_2)T_s$

$$d_2 = \frac{v_{in}}{v_C - v_{in}} \cdot d_1. \quad (17)$$

The piecewise linear model for the capacitor voltage is

$$\frac{dv_C}{dt} = \begin{cases} -\frac{v_C}{RC} & t \in [0, d_1 T_s] \\ \frac{i_L}{C} - \frac{v_C}{RC} & t \in [d_1 T_s, (d_1 + d_2) T_s] \\ -\frac{v_C}{RC} & t \in [(d_1 + d_2) T_s, T_s] \end{cases} \quad (18)$$

which, upon substitution by (16) and (17) and averaging over a switching cycle, becomes

$$\begin{aligned} \frac{d\bar{v}_C}{dt} &= \frac{1}{T_s} \int_{d_1 T_s}^{(d_1 + d_2) T_s} \left( \frac{\bar{v}_{in} d_1 T_s}{LC} - \frac{\bar{v}_C - v_{in}}{LC} \cdot t \right) dt - \frac{\bar{v}_C}{RC} \\ &= \frac{v_{in}^2}{2LC} \cdot \frac{d_1^2 T_s}{\bar{v}_C - v_{in}} - \frac{\bar{v}_C}{RC}. \end{aligned}$$

This is exactly the same as the conventional reduced-order model (15). The application of this method to other types of converters, such as quasiresonant converters, can be tedious because of the complicated and lengthy algebra involved. To solve this problem, a symbolic analysis program package has been developed that can generate the averaged model automatically from a netlist of the converter topology and some other simple inputs describing the operation of the converter [9], [10].

### III. NEW FULL-ORDER AVERAGED MODELS

The reduced-order averaged model can correctly predict the dc and low-frequency behavior of PWM DCM converters. At high frequencies, small-signal response measurement (to be presented in the next section) clearly shows second-order (for second-order topologies such as boost and buck) dynamics that the reduced-order model is unable to capture. The large discrepancy of the reduced-order model at high frequencies may not be acceptable for some applications that require high performance control. Full-order averaged models that can correctly predict high-frequency responses are therefore desired. From a theoretical standpoint, many researchers in the field had been puzzled by the fact that averaged models in CCM can be accurate up to one third of the switching frequency, while a seemingly similar averaging technique leads to inaccurate models in DCM. These are some of the motivations for seeking new full-order averaged models for DCM PWM converters.

#### A. Model Derivation

The derivation of a full-order model starts from the modified averaged model (9). Unlike the conventional approach that relies on the volt-second balance relation for the definition of  $d_2$ , a different duty-ratio constraint will be derived here. Equation (5), which is repeated below for easy reference, can be used for this purpose

$$\bar{i}_L = \frac{i_{pk}}{2} \cdot (d_1 + d_2).$$

Assume that the voltage across the inductor is  $v_{on}$  when the switch is on (during  $[0, d_1 T_s]$ ), the inductor peak current can be written as

$$i_{pk} = \frac{v_{on}}{L} \cdot d_1 T_s. \quad (19)$$

Substituting this into (5) and solving the resulting equation for  $d_2$  yields

$$d_2 = \frac{2L\bar{i}_L}{d_1 T_s v_{\text{on}}} - d_1 \quad (20)$$

which is different from the result based on the volt-second balance relation because it enforces the correct average charging of the output capacitor. The duty-ratio constraint (20) can be substitute into (9) to generate a full-order averaged model.

As example, we consider the boost converter again. When the switch is on, the voltage across the inductor in boost converter is  $v_{\text{in}}$ . Hence the new duty-ratio constraint for boost converter is

$$d_2 = \frac{2L\bar{i}_L}{d_1 T_s v_{\text{in}}} - d_1. \quad (21)$$

Notice that this expression balances both flux and charge as the converter operates. Substituting this into (10) gives the following full-order averaged model for boost converter in DCM:

$$\frac{d\bar{i}_L}{dt} = \frac{2\bar{i}_L}{d_1 T_s} \left(1 - \frac{\bar{v}_C}{v_{\text{in}}}\right) + \frac{d_1 \bar{v}_C}{L} \quad (22)$$

$$\frac{d\bar{v}_C}{dt} = \frac{\bar{i}_L}{C} - \frac{d_1^2 T_s v_{\text{in}}}{2LC} - \frac{\bar{v}_C}{RC}. \quad (23)$$

### B. DC Analysis

The dc operating point of the boost converter with a constant duty ratio  $d_1 = D_1$  can be determined by letting the right-hand sides of differential equations (22) and (23) equal to zero and solving the two resulting algebraic equations for  $\bar{i}_L$  and  $\bar{v}_C$ . Let the scalar value of  $M$  be the intended output–input voltage ratio. The results can be expressed as

$$M = \frac{\bar{V}_C}{V_{\text{in}}} = \frac{1}{2} + \frac{1}{2} \sqrt{1 + \frac{2D_1^2 R}{L f_s}}$$

$$\bar{I}_L = \frac{D_1^2 V_{\text{in}} M}{2L f_s (M - 1)}.$$

It can be verified that this represents the same dc operating point as that predicted by the conventional reduced-order model [3], [4] as well as by the previous full-order model [5], [6].

### C. Small-Signal Linear Model

Using standard linearization techniques, a small-signal model can be derived from (22) and (23) as follows:

$$\frac{d}{dt} \begin{bmatrix} \hat{i}_L \\ \hat{v}_C \end{bmatrix} = A \begin{bmatrix} \hat{i}_L \\ \hat{v}_C \end{bmatrix} + B \begin{bmatrix} \hat{v}_{\text{in}} \\ \hat{d}_1 \end{bmatrix} \quad (24)$$

where

$$A = \begin{bmatrix} \frac{2(1-M)}{D_1 T_s} & -\frac{2M}{D_1 R T_s} \\ \frac{1}{C} & -\frac{1}{RC} \end{bmatrix}, \quad B = \begin{bmatrix} \frac{M^2}{L(M-1)} & \frac{2M V_{\text{in}}}{L} \\ -\frac{D_1^2 T_s}{2LC} & -\frac{D_1 T_s V_{\text{in}}}{LC} \end{bmatrix}.$$

Various transfer functions can be determined from this small-signal model. The control-to-output transfer function, for example, is obtained as

$$\frac{\hat{V}_C(s)}{\hat{D}_1(s)} = \frac{K \left( \frac{2}{D_1 T_s} - s \right)}{s^2 + \left[ \frac{1}{RC} + \frac{2(M-1)}{D_1 T_s} \right] s + \frac{2(2M-1)}{D_1 T_s RC}}$$

$$\approx \frac{K \left( \frac{2}{D_1 T_s} - s \right)}{\left[ s + \frac{2M-1}{(M-1)RC} \right] \left[ s + \frac{2(M-1)}{D_1 T_s} \right]} \quad (25)$$

where  $K$  is a constant. The approximation in the above expression holds under the assumption that

$$\frac{2(M-1)}{D_1 T_s} \gg \frac{1}{RC}$$

which will hold under conditions of low output ripple.

### D. New Full-Order Model for Other Basic Topologies

Based on (5) and (19), new duty-ratio constraints and, consequently, new full-order averaged models can also be derived for other topologies. The results for buck, boost, and buck-boost converters are given below for easy reference.

#### 1) Buck

$$\frac{d\bar{i}_L}{dt} = \frac{d_1 v_{\text{in}}}{L} - \frac{2\bar{i}_L \bar{v}_C}{d_1 T_s (v_{\text{in}} - \bar{v}_C)} \quad (26)$$

$$\frac{d\bar{v}_C}{dt} = \frac{\bar{i}_L}{C} - \frac{\bar{v}_C}{RC}. \quad (27)$$

#### 2) Boost

$$\frac{d\bar{i}_L}{dt} = \frac{2\bar{i}_L}{d_1 T_s} \left(1 - \frac{\bar{v}_C}{v_{\text{in}}}\right) + \frac{d_1 \bar{v}_C}{L} \quad (28)$$

$$\frac{d\bar{v}_C}{dt} = \frac{\bar{i}_L}{C} - \frac{d_1^2 T_s v_{\text{in}}}{2LC} - \frac{\bar{v}_C}{RC}. \quad (29)$$

#### 3) Buck-Boost

$$\frac{d\bar{i}_L}{dt} = \frac{d_1 (v_{\text{in}} + \bar{v}_C)}{L} - \frac{2\bar{i}_L \bar{v}_C}{d_1 v_{\text{in}} T_s} \quad (30)$$

$$\frac{d\bar{v}_C}{dt} = \frac{\bar{i}_L}{C} - \frac{d_1^2 T_s v_{\text{in}}}{2LC} - \frac{\bar{v}_C}{RC}. \quad (31)$$

The discussion so far has focused on DCM operation involving the inductor. The proposed modeling procedure is also applicable to DCM operation involving the capacitor or multiple inductors [5] which would occur in high-order topologies such as Cuk, Sepic, and Zeta. As an example, consider the Cuk converter depicted in Fig. 2. Three different discontinuous conduction modes can occur in this converter:

- 1)  $i_{L_1} + i_{L_2}$  is discontinuous (during the off period of the switch);
- 2) both  $i_{L_1}$  and  $i_{L_2}$  are discontinuous;
- 3)  $v_{C_1}$  is discontinuous (in which case the switch and the diode are on simultaneously).

The proposed modeling procedure is directly applicable to case 1) and 2), although the derivation in case 2) is more tedious. The third case would occur when the internal transfer capacitor  $C_1$  is small. A full-order averaged model can be derived for it by using

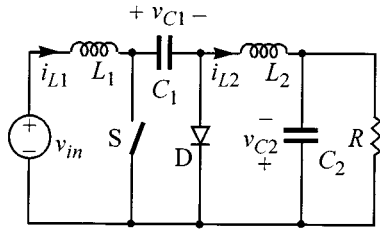


Fig. 2. Cuk converter topology.

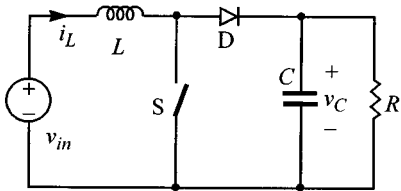


Fig. 3. Boost converter with resistive load.

the proposed modeling procedure and the following duty-ratio constraint ( $d'_1 = 1 - d_1, d'_2 = 1 - d_2$ ):

$$d'_2 = \frac{2\bar{v}_{C1}C_1}{d'_1T_s\bar{i}_{L2}} - d'_1. \quad (32)$$

Note the duality between (32) and (20). Detailed analysis of DCM in high-order topologies will be addressed in future work.

#### IV. MODEL COMPARISON AND VERIFICATION

##### A. Model Comparison

In this section, the new full-order averaged models are compared with the reduced-order models and the full-order averaged models presented in [5] and [6]. For the boost converter, the full-order averaged model derived using the method presented in [5] and [6] is

$$\frac{d\bar{i}_L}{dt} = \frac{v_{in}}{L} - \frac{2\bar{i}_L\bar{v}_C}{d_1^2T_s\bar{v}_C + 2L\bar{i}_L} \quad (33)$$

$$\frac{d\bar{v}_C}{dt} = \frac{2L\bar{i}_L^2}{C(d_1^2T_s\bar{v}_C + 2L\bar{i}_L)} - \frac{\bar{v}_C}{RC}. \quad (34)$$

The comparison is made at the small-signal level. Table II summarizes the poles and the zero in the control-to-output transfer function of the boost converter predicted by the three different models (15), (33), (34), and (22), (23). The reduced-order model does not include the second pole or the right-half-plane (RHP) zero. There is also a significant difference between the second poles and the RHP zeros predicted by the new model and the previous full-order model. Table III shows the poles and zeros of the control-to-output transfer function for buck and buck-boost converters predicted by the new model.

##### B. Model Verification

To verify the accuracy of the new model against previous models, a boost converter with the following parameters was designed:  $L = 5 \mu\text{H}$ ,  $C = 40 \mu\text{F}$ ,  $f_s = 100 \text{ kHz}$  ( $T_s = 10 \mu\text{s}$ ),  $V_g = 5 \text{ V}$ , and  $R = 20 \Omega$ . The converter was first simulated with a detailed switching model using SABER [12]. ESR's of both

TABLE II  
COMPARISON OF POLE AND ZERO LOCATIONS FOR THE BOOST CONVERTER

Model	1st Pole $s_{p1}$	2nd Pole $s_{p2}$	RHP Zero $s_z$
Model (15)	$\frac{2M-1}{M-1} \cdot \frac{1}{RC}$	none	none
Model (33)-(34)	$\frac{2M-1}{M-1} \cdot \frac{1}{RC}$	$\frac{2(M-1)^2}{D_1^2M^2T_s}$	$\frac{2(M-1)}{D_1^2MT_s}$
New Model (22)-(23)	$\frac{2M-1}{M-1} \cdot \frac{1}{RC}$	$\frac{2(M-1)}{D_1T_s}$	$\frac{2}{D_1T_s}$

TABLE III  
NEW POLE AND ZERO LOCATIONS FOR BUCK AND BUCK-BOOST CONVERTERS

Converter	1st Pole $s_{p1}$	2nd Pole $s_{p2}$	RHP Zero $s_z$
Buck	$\frac{2-M}{1-M} \cdot \frac{1}{RC}$	$\frac{2M}{D_1(1-M)T_s}$	none
Buck-Boost	$\frac{2}{RC}$	$\frac{2M}{D_1T_s}$	$\frac{2}{D_1T_s}$

the inductor and the capacitor are taken into account in the simulation in order to match the experimental set-up. Fig. 4 shows the simulated small-signal control-to-output ( $\hat{V}_0(s)/\hat{D}_1(s)$ ) response in the frequency domain. For comparison, the corresponding responses predicted by the new and the two previous models are also shown. As the figure shows, the new averaged model gives the most accurate response compared to detailed simulation. The response is almost identical to that of the detailed switching model in the frequency range up to one third of the switching frequency. The improvement of the new model over previous models is significant, especially in the phase response.

Simulated frequency responses above one third of the switching frequency are not included in Fig. 4. This is because the converter response is dependent on the phase of the disturbance, and this sensitivity cannot be picked up with any average-based LTI model. The phase dependency becomes especially significant above about 1/3 of the switching frequency. For example, a sine disturbance in  $d_1$  at half the switching frequency produces a same-frequency output component that lags the disturbance by  $141.5^\circ$  and has a magnitude of  $0.568 \text{ V}$  (corresponding to  $-4.9 \text{ dB}$ ). A cosine disturbance at the same frequency produces a phase angle of  $-230^\circ$  and magnitude of  $34.7 \text{ mV}$  ( $-29.2 \text{ dB}$ ).

Measured control-to-output frequency response of the converter at  $D_1 = 0.7$  is compared in Fig. 5 with predictions of the new full-order averaged model. The losses of the converter were addressed in the model by a  $0.4 \Omega$  resistor in series with the inductor, which accounts for the reduction of the dc gain compared to the simulation results. As the figure shows, the new model predicts almost exactly the same response as the experiments up to one third of the switching frequency, at which point the disturbance phase effect begins to be significant.

#### V. DELAY EFFECT AND DUTY-RATIO CONSTRAINTS

The numerical and experimental results in the previous section clearly showed the improved accuracy of the new model over previous models. The results, however, do not explain why the new models are more accurate. More analytical results are

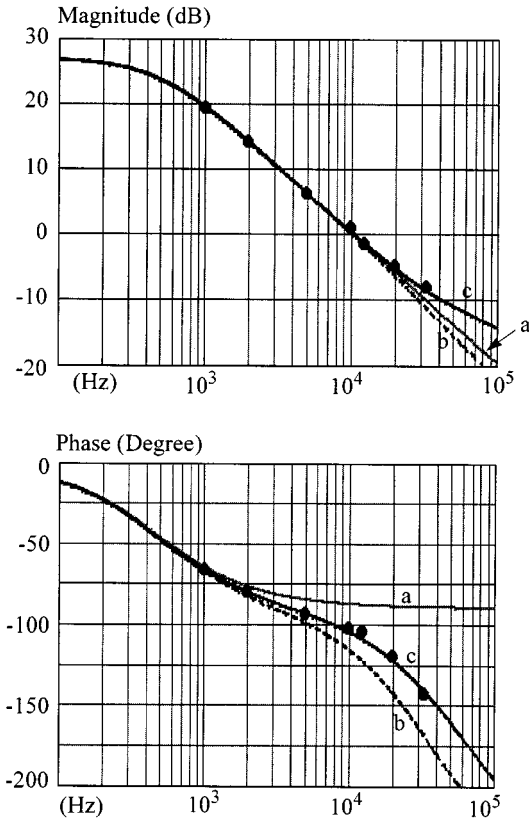


Fig. 4. Control-to-output frequency responses of the DCM boost converter predicted by (a) model (15), (b) model (33) and (34), and (c) the new model (22), (23). The dots represent switching model simulation results obtained using SABER.

provided in this section to further explain the differences and relationships among the various models as we strive to understand the dynamic behavior of DCM operation in general.

First, we want to point out that averaged modeling of PWM converters in DCM involves two steps at which approximations are introduced: the determination of the dependent duty ratio  $d_2$ , and the averaging process. This is in contrast to the CCM case, in which only averaging is involved. It is possible to quantify the error introduced by averaging. In the CCM case, it is generally believed that averaging does not introduce significant error as long as the switching frequency is sufficiently higher than the natural frequency of the converter, and the averaged model can be expected to be accurate up to one third of the switching frequency. The degree of error can be analyzed more explicitly [7], and the perception is generally true. In the DCM case, we would expect similar accuracy of the averaged model if we could find an “exact” expression for  $d_2$ . In other words, the unusually large discrepancies (compared to CCM case) exhibited by previous DCM models can largely be attributed to the use of inaccurate constraints that define  $d_2$ .

Second, we note that all models compared in the last section predict the same dc as well as low-frequency responses. The differences and discrepancies exist only at high frequencies. Since the inductor current in DCM resets to zero (or a constant) in every switching cycle, the energy flow in the inductor is independent from cycle to cycle, i.e., the inductor does not carry any *information* from cycle to cycle. From this standpoint, one could

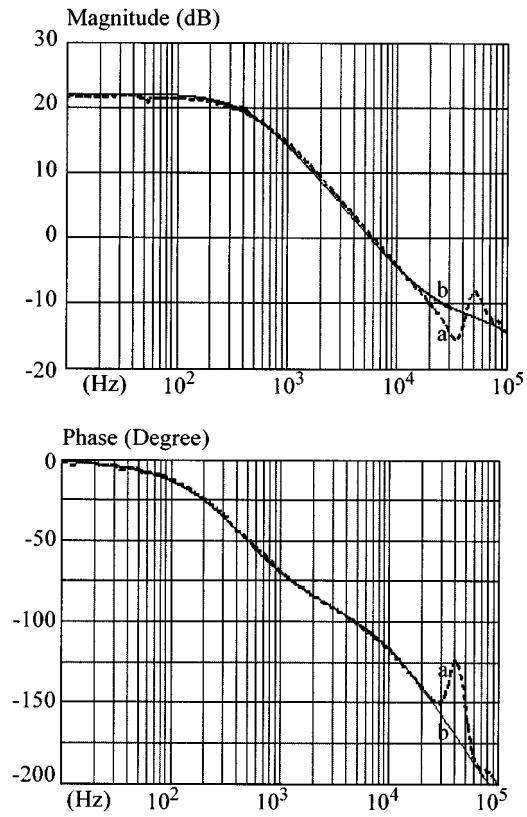


Fig. 5. Measured control-to-output frequency responses of the DCM boost converter in comparison with predictions by the new averaged model. Dashed lines (a) measurements; solid lines and (b) model predictions.

argue that the inductor current no longer acts as a state variable. However, within each switching cycle, the inductor current is still a dynamic variable and does contribute to the fast dynamics of the converter. Previous models failed to accurately capture these fast dynamics, hence are unable to predict converter responses at high frequencies.

#### A. The Fast Dynamics

To understand the origin of the fast dynamics associated with the inductor current, we assume that input and output voltages are kept constant. Under this assumption, the inductor current has a constant slope in both subintervals  $[0, d_1 T_s]$  and  $[d_1 T_s, (d_1 + d_2) T_s]$ . The steady-state waveform of the current is shown in Fig. 6(a), while *b* and *c* illustrate the duty ratios of the two subintervals. Now consider that a small-signal disturbance,  $\hat{d}_1$ , is added to  $d_1$ , as shown in Fig. 6(d). As the result, the inductor current will also be perturbed, as shown in Fig. 6(a) by the dashed line. The current perturbation,  $\hat{i}_L$ , starts from zero at  $t = D_1 T_s$ , reaches the peak at  $t = (D_1 + \hat{d}_1) T_s$ , and resets to zero at  $t = (D_1 + D_2 + \delta) T_s$ , as illustrated by Fig. 6(g). Based on the waveform, the shift,  $\delta$ , of the trailing edge of the second subinterval, and the peak of the perturbation  $\hat{i}_L$  can be calculated as follows:

$$\hat{i}_L[(D_1 + \hat{d}_1) T_s] = \hat{i}_L[(D_1 + D_2) T_s] = \frac{V_{\text{on}} + V_{\text{off}}}{L} \cdot \hat{d}_1 T_s \quad (35)$$

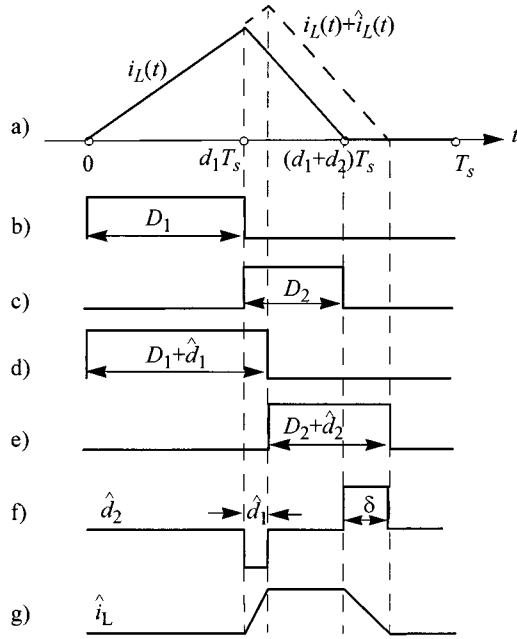


Fig. 6. Small-signal dynamics of inductor current.

$$\frac{V_{\text{off}}}{L} \cdot \delta T_s = \hat{i}_L [(D_1 + D_2)T_s] \Rightarrow \delta = \left(1 + \frac{V_{\text{on}}}{V_{\text{off}}}\right) \cdot \hat{d}_1. \quad (36)$$

$V_{\text{on}}$  and  $V_{\text{off}}$  are the voltages across the inductor when the switch or the diode conducts the current, respectively. Their reference directions are taken such that both are positive.

Based on (35) and (36) as well as the waveform in Fig. 6(g), the Laplace transform of  $\hat{i}_L$  can now be determined as follows [11]:

$$\begin{aligned} \hat{I}_L(s) &= \frac{1}{T_s} \int_0^{\infty} \hat{i}_L(t) e^{-st} dt = \frac{1}{T_s} \int_0^{D_2 T_s} \hat{i}_L(t) e^{-st} dt \\ &= \frac{V_{\text{on}} + V_{\text{off}}}{L} \cdot \hat{d}_1 \cdot \frac{1 - e^{-D_2 T_s s}}{s}. \end{aligned} \quad (37)$$

Therefore, the transfer function from a perturbation in  $d_1$  to the corresponding perturbation in  $i_L$  is

$$\frac{\hat{I}_L(s)}{\hat{D}_1(s)} = \frac{V_{\text{on}} + V_{\text{off}}}{L} \cdot \frac{1 - e^{-D_2 T_s s}}{s} \quad (38)$$

which, upon Pade approximation [13] of the exponential function, can be expanded as

$$\frac{\hat{I}_L(s)}{\hat{D}_1(s)} = \frac{V_{\text{on}} + V_{\text{off}}}{L} \cdot \frac{D_2 T_s}{1 + \frac{D_2 T_s s}{2}}. \quad (39)$$

It can be concluded from (39) that *the effect of the fast dynamics associated with the inductor current in DCM is to introduce a high-frequency pole at  $s_p = 2/(D_2 T_s)$* . It can be verified that this is the same high-frequency pole predicted by the new full-order model for the three basic converter topologies.

## B. Delay Effect

As Fig. 6(e) shows, the effect of the perturbation  $\hat{d}_1$  is to delay the leading edge of  $d_2$  by  $\hat{d}_1 T_s$  and extend its trailing edge by  $\delta T_s$ . Therefore, the total change in  $d_2$  as a result of  $\hat{d}_1$  is

$$\hat{d}_2 = \delta - \hat{d}_1 = \left(1 + \frac{V_{\text{on}}}{V_{\text{off}}}\right) \cdot \hat{d}_1 - \hat{d}_1 = \frac{V_{\text{on}}}{V_{\text{off}}} \cdot \hat{d}_1. \quad (40)$$

However, this expression does not take into account the sequence of changes: As can be seen from Fig. 6(e), as  $d_1$  is increased at  $D_1 T_s$  by  $\hat{d}_1$ ,  $d_2$  drops immediately by the same amount, and then increases by  $\delta$  after a delay time  $D_2 T_s$ . Taking this delay into account,  $\hat{d}_2$  shall be written as  $\hat{d}_2 = -\hat{d}_1 + \delta \cdot u(t - D_2 T_s)$ , where  $u(t - D_2 T_s)$  is a unit step function, and its Laplace transform

$$\begin{aligned} \hat{D}_2(s) &= -\hat{D}_1(s) + \delta e^{-D_2 T_s s} \\ &= \left[-1 + \left(1 + \frac{V_{\text{on}}}{V_{\text{off}}}\right) \cdot e^{-D_2 T_s s}\right] \hat{D}_1(s). \end{aligned} \quad (41)$$

This relation can also be approximated as follows by using the Pade expansion

$$\frac{\hat{D}_2(s)}{\hat{D}_1(s)} = -1 + \left(1 + \frac{V_{\text{on}}}{V_{\text{off}}}\right) \cdot \frac{1 - \frac{D_2 T_s s}{2}}{1 + \frac{D_2 T_s s}{2}}. \quad (42)$$

We demonstrate now that the fast dynamics associated with the inductor current can also be determined by using (41) in combination with the averaged model of the inductor. For this purpose, note that the averaged model of the inductor can be written as

$$L \frac{d\hat{i}_L}{dt} = d_1 v_{\text{on}} - d_2 v_{\text{off}}. \quad (43)$$

Under the assumption of constant  $v_{\text{on}} (= V_{\text{on}})$  and  $v_{\text{off}} (= V_{\text{off}})$ , this model can be transformed into the frequency domain as

$$Ls \hat{I}_L(s) = V_{\text{on}} \hat{D}_1(s) - V_{\text{off}} \hat{D}_2(s) \quad (44)$$

which, upon substitution of  $\hat{D}_2(s)$  with (41), becomes the same as (38). In contrast, substituting (40) into (43) yields  $\hat{I}_L(s)/\hat{D}_1(s) = 0$ , which corresponds to the conventional reduced-order model and does not correctly predict the dynamics of  $i_L$ .

## C. Duty-Ratio Constraints

Now we turn back to our original question of why the new duty-ratio constraint (20) would result in more accurate models. From the above discussion, we conclude that the correct constraint should allow the delay effect to be incorporated. Note that the small-signal relations (41) and (42) do not provide a large-signal constraint on  $d_2$ . But the large-signal constraint should simplify to (41) or (42) upon linearization (under the assumption of constant input and output voltages).

The new model as well as the models presented in [3] and [5] have been reexamined by comparing the corresponding duty-ratio constraint against (42). The analysis was done by assuming constant input and output voltages and calculating both transfer functions  $\hat{I}_L(s)/\hat{D}_1(s)$  and  $\hat{D}_2(s)/\hat{D}_1(s)$ . It was found (and can be readily verified) that the new model gives

exactly the same transfer functions as (39) and (42) under this condition. The constraint used in deriving the reduced-order model is  $d_1 v_{\text{on}} = d_2 v_{\text{off}}$  which effectively eliminates the fast dynamics, as can be seen from the last subsection. For the averaged switch model presented in [6], the transfer function  $\hat{D}_2(s)/\hat{D}_1(s)$  under constant terminal voltage condition is found to be

$$\frac{\hat{D}_2(s)}{\hat{D}_1(s)} = \frac{V_{\text{on}}}{V_{\text{off}}} \cdot \left[ 1 - \frac{D_1^2 T_s s}{2} \left( 1 + \frac{D_2}{D_1} \right)^2 \right] \cdot \left[ 1 + \frac{D_1^2 T_s s}{2} \left( 1 + \frac{D_2}{D_1} \right)^2 \right]^{-1}.$$

This is again different from (42) which explains why the resulting model predicts inaccurate high-frequency poles. In addition, another constraint used in [14], which is also based on (5) but calculates  $i_{pk}$  from the second subinterval, i.e.,

$$\bar{i}_L = \frac{i_{pk}}{2} \cdot (d_1 + d_2) = \frac{v_{\text{off}}}{2L} \cdot d_2 T_s (d_1 + d_2) \quad (45)$$

was also analyzed, and the following transfer functions were obtained:

$$\frac{\hat{D}_2(s)}{\hat{D}_1(s)} = \frac{V_{\text{on}}}{V_{\text{off}}} \cdot \frac{(1 - \frac{D_1 T_s s}{2})}{1 + (\frac{D_1}{2} + D_2) T_s s},$$

$$\frac{\hat{I}_L(s)}{\hat{D}_1(s)} = \frac{V_{\text{on}} + V_{\text{off}}}{L} \cdot \frac{D_2 T_s}{1 + (\frac{D_1}{2} + D_2) T_s s}.$$

They again differ from (39) and (42). Therefore, we can expect the model presented in [14] also to predict inaccurate response at high frequencies [15].

In summary, PWM converters operating in DCM exhibit fast dynamics due to the transient behavior of the inductor current within a switching cycle. The constraint defining  $d_2$  is the key to accurate prediction of these fast dynamics with averaged models. The constraint (20) proposed in this paper results in accurate averaged models because it correctly captures the fast dynamics associated with the inductor current. All averaged models have limited utility above about one third of the switching frequency, since the response above that value depends on the specific timing of the disturbance and is not captured with a conventional frequency-domain model.

## VI. AVERAGED SWITCH MODEL

There are instances where it is desirable to represent the averaged model by an equivalent circuit so that it can be implemented in a simulation program or embedded in a larger system. For example, large-signal stability analysis of a distributed power system usually relies on averaged model simulation of the system. To serve those applications, the averaged circuit counterpart of the new full-order averaged model is developed in this section.

The idea of averaged circuit modeling is to identify a switch cell that is common in different topologies and to develop an equivalent circuit that, when inserted in place of the original switch cell, results in an electrical circuit that has the same average behavior as the converter. The switch cell identified here

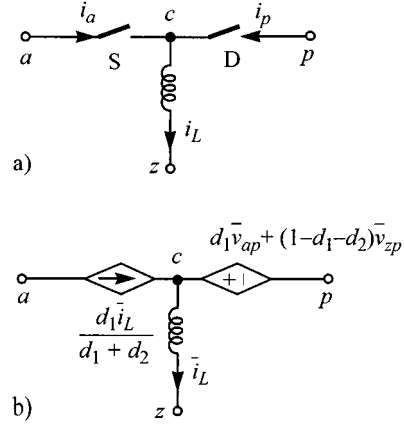


Fig. 7. (a) Three-terminal PWM switch cell and (b) its average model for DCM operation.

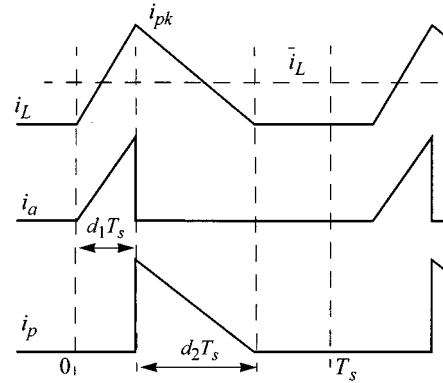


Fig. 8. Terminal current waveform of the switch cell defined in Fig. 7.

includes the switch, the diode, and the inductor, as shown in Fig. 7(a). It is suitable for converters with current-based discontinuous modes. Fig. 8 shows the waveform of the currents at the three terminals of this cell when the inductor current is in DCM. The following relations can be found between the instantaneous values of the terminal voltages and currents over a switching cycle:

$$i_a = \begin{cases} i_L & t \in [0, d_1 T_s] \\ 0 & t \in [d_1 T_s, (d_1 + d_2) T_s] \\ 0 & t \in [(d_1 + d_2) T_s, T_s] \end{cases} \quad (46)$$

$$v_{cp} = \begin{cases} v_{ap} & t \in [0, d_1 T_s] \\ 0 & t \in [d_1 T_s, (d_1 + d_2) T_s] \\ v_{zp} & t \in [(d_1 + d_2) T_s, T_s]. \end{cases} \quad (47)$$

From these the following equations relating average terminal voltages and currents can be deduced:

$$\bar{i}_a = d_1 \bar{i}_L, \quad \bar{v}_{cp} = d_1 \bar{v}_{ap} + (1 - d_1 - d_2) \bar{v}_{zp}. \quad (48)$$

These relations can be represented by the circuit shown in Fig. 7(b). The model is completed by the duty-ratio constraint (20) which is rewritten using variables defined for the switch cell

$$d_2 = \frac{2L \bar{i}_L}{\bar{v}_{az} d_1 T_s} - d_1. \quad (49)$$

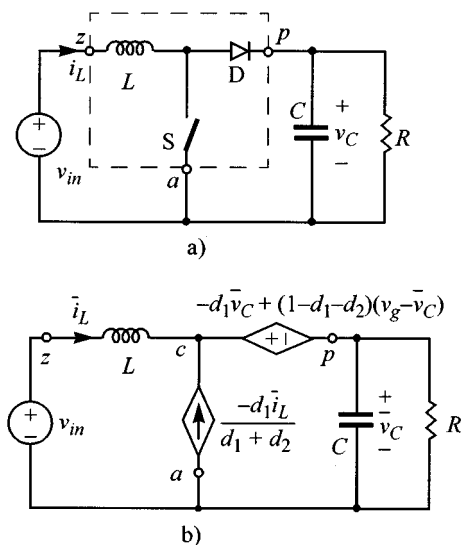


Fig. 9. (a) PWM boost converter and (b) its averaged circuit model for DCM.

The combination of (48) and (49) addresses averaging fundamentally as in (5) and (6). We use again the boost converter as example to demonstrate the use of this averaged switch model. Point-by-point substitution of the switch cell, as enclosed in the dashed line in Fig. 9(a), with the averaged switch model shown in Fig. 7(b) yields the averaged circuit model of Fig. 9(b). It is straightforward to verify that the state-space model of the averaged circuit is the same as (22) and (23).

## VII. CONCLUSION

Various aspects of averaged modeling of PWM converters in discontinuous conduction mode have been studied in this paper. The proposed modeling procedure consists of

- 1) averaging;
- 2) inductor current or capacitor voltage representation;
- 3) an algebraic duty-ratio constraint.

Among these, the duty-ratio constraint has received the least attention in previous work but is found to be the key to accurate prediction of high-frequency behavior. The proposed procedure is streamlined and provides a general framework in which different models can be compared.

A new duty-ratio constraint is proposed, based on formal averaging, which leads to new full-order averaged models that are different from previous ones. Numerical simulation and experimental measurement of a boost converter confirm that the new model correctly predicts the small-signal response up to the maximum frequency that can be addressed with a linear time-invariant frequency domain model, while previous models are only good under about one tenth of the switching frequency. Small-signal models (poles and zeros) predicted by the new procedure are tabulated for basic converter topologies for easy reference.

To fully understand DCM dynamics and the differences among various models, efforts have been made to identify the origin of the high-frequency pole which distinguishes the different models. As the result, a time delay is useful to properly

model the small-signal response, and the high-frequency pole is shown to correspond to this delay. The delay effect is correctly captured by the new duty-ratio constraint. In contrast, previous models are not able to predict the high-frequency pole because the duty-ratio constraints used there do not capture the delay effect.

For applications such as large-signal stability analysis of distributed power systems, an averaged switch model that corresponds to the new full-order averaged models is presented. The switch cell includes the switch, the diode, and the discontinuous-mode inductor, and is common to different PWM converter topologies. The corresponding averaged switch model is obtained by replacing the switch and diode with a controlled current and voltage source, respectively. The duty-ratio constraints used in defining these controlled sources are the same as those used in the analytical models.

## ACKNOWLEDGMENT

The authors wish to dedicate this paper to the memory of their late co-author and colleague, Dr. R. M. Bass, whose untimely death was a great sadness felt by all of them.

## REFERENCES

- [1] D. Weng and S. Yuvarajan, "Constant-switching frequency ac-dc converter using second-harmonic-injection PWM," in *Proc. APEC'95*, 1995, pp. 642–646.
- [2] J. Sun, N. Froelcke, and H. Grotstollen, "Harmonic reduction techniques for single-switch three-phase boost rectifiers," in *Proc. IAS'96*, 1996, pp. 1225–1232.
- [3] S. Cuk and R. D. Middlebrook, "A general unified approach to modeling switching DC-to-DC converters in discontinuous conduction mode," in *Proc. IEEE PESC'77*, 1977, pp. 36–57.
- [4] R. Tymerski and V. Vorperian, "Generation, classification and analysis of switched-mode DC-to-DC converters by the use of converter cells," in *Proc. INTELEC'86*, Oct. 1986, pp. 181–195.
- [5] D. Maksimovic and S. Cuk, "A unified analysis of PWM converters in discontinuous modes," *IEEE Trans. Power Electron.*, vol. 6, pp. 476–490, May 1991.
- [6] V. Vorperian, "Simplified analysis of PWM converters using model of PWM switch, Part II: Discontinuous conduction mode," *IEEE Trans. Aerosp. Electron. Syst.*, vol. 26, pp. 497–505, May 1990.
- [7] P. T. Krein, J. Bentsman, R. M. Bass, and B. C. Lesieutre, "On the use of averaging for the analysis of power electronic systems," *IEEE Trans. Power Electron.*, vol. 5, pp. 182–190, July 1990.
- [8] J. Sun and H. Grotstollen, "Averaged modeling of switching power converters: reformulation and theoretical basis," in *Proc. IEEE PESC'92*, 1992, pp. 1166–1172.
- [9] —, "Symbolic analysis methods for averaged modeling of switching power converters," *IEEE Trans. Power Electron.*, vol. 12, pp. 537–546, May 1997.
- [10] J. Sun, D. M. Mitchell, M. Greuel, P. T. Krein, and R. M. Bass, "Averaged modeling of PWM converters in discontinuous conduction mode: A reexamination," in *Proc. IEEE PESC'98*, 1998, pp. 615–622.
- [11] D. Maksimovic, "Automated small-signal analysis of switching converters using a general-purpose time-domain simulator," in *Proc. IEEE APEC'98 Conf.*, 1998, pp. 357–362.
- [12] *SABER Designer Reference*, Analogy, Inc., Beaverton, OR, 1996.
- [13] W. Press *et al.*, *Numerical Recipes in C*, 2nd ed. Cambridge, U.K.: Cambridge Univ. Press, 1992.
- [14] Y. Amran, F. Huliehel, and S. Ben-Yaakov, "A unified SPICE compatible average model of PWM converters," *IEEE Trans. Power Electron.*, vol. 6, pp. 585–594, July 1991.
- [15] S. Ben-Yaakov and D. Adar, "Average models as tools for studying the dynamics of switch mode DC-DC converters," in *Proc. PESC'94*, 1994, pp. 1369–1376.



**Jian Sun** (M'95) received the B.S.E.E. degree from the Nanjing Institute of Aeronautics, Nanjing, China, in 1984, the M.S.E.E. degree from the Beijing University of Aeronautics and Astronautics, Beijing, China, in 1989, and the Dr.Eng. degree from the University of Paderborn, Germany, in 1995.

From 1984 to 1987, he worked in the R&D Center, Xian Aircraft Company, Xian, China, where he was involved in the design of aircraft electrical power systems. He worked in the Institute for Power Electronics and Electrical Drives, University of Paderborn, from 1991 to 1996, first as a Research Assistant, and then as a Research Associate while pursuing his doctoral degree. He was a Post-Doctoral Fellow with the School of Electrical and Computer Engineering, Georgia Institute of Technology, Atlanta, from 1996 to 1997, where he taught undergraduate courses on electromechanical energy conversion in addition to conducting research on dc/dc and ac/dc converters. He joined the Advanced Technology Center, Rockwell Collins, Cedar Rapids, IA, in 1997, where he is currently a Principal Engineer and the leader for research in power electronics. He has published more than 30 papers at various IEEE conferences and journals. His research interests are in the areas of power converter topologies, soft-switching techniques, system modeling and analysis, magnetic components and high density, high efficiency dc/dc, and ac/dc converters.



**Daniel M. Mitchell** (M'76–SM'79) was born in Denver, CO, on November 8, 1938. He received the B.S.E.E. degree from the Massachusetts Institute of Technology, Cambridge, in 1960 and the M.S.E.E. degree from Iowa State University, Ames, in 1966.

From 1960 to 1963, he was with the Westinghouse Research and Development Laboratories, Pittsburgh, PA, where he assisted in the development of variable-frequency, solid-state induction motor drives. From 1963 to 1967, he was with the Collins Radio Company, Cedar Rapids, IA, where he designed signal conditioning equipment for the Apollo program and was a power supply design engineer. In 1967, he joined the Hallicrafters division of Northrop Corporation, Chicago, IL, where he designed prototype high power switching regulators and pulse modulators for infrared countermeasure systems. In 1968, he returned to Collins Radio, which became the Collins Division of Rockwell International Corporation in 1974, where his principal activity was the design and development of state-of-the-art military power supplies. He entered management in 1983 and retired in 1998 as head of the Advanced Subsystems and Signal Processing Department, Rockwell Collins Advanced Technology Center, where he had responsibility for core technology groups in the areas of power conversion, frequency synthesizers, frequency standards, and digital/optical signal processing. He is currently doing business as DM Mitchell Consultants, specializing in power conversion design, analysis and education. He has authored numerous papers and magazine articles, including six IEEE Power Electronics Society TRANSACTIONS papers. He has been issued twelve patents. Beginning in 1988 he has given over 50 public and in-house short courses on power supply design and analysis. He was an Adjunct Instructor at the University of Iowa, Iowa City, from 1983 until his retirement, teaching a senior/graduate course in power electronics that he developed. He is Past Chairman of the Rockwell Corporate Technical Panel on Power Conversion and has authored the textbook *DC–DC Switching Regulator Analysis* (New York: McGraw-Hill, 1988).

Mr. Mitchell was named Rockwell Collins Engineer of the Year in 1980.



**Matthew F. Greuel** received the B.S. degree in electrical engineering from the University of Illinois, Urbana, in 1995.

He is an Engineering Supervisor for R.R. Donnelley and Sons, Mattoon, IL. His interests are machine control, variable frequency motor drives, and dc–dc converter control.



**Philip T. Krein** (S'76–M'82–SM'93–F'00) received the B.S. degree in electrical engineering and the A.B. degree in economics from Lafayette College, Easton, PA, and the M.S. and Ph.D. degrees in electrical engineering from the University of Illinois, Urbana.

He was an Engineer with Tektronix, Inc., Beaverton, OR, with responsibilities in analog design and product development, then returned to the University of Illinois, where he is now Professor of Electrical and Computer Engineering. He is also Director of the Grainger Center for Electric

Machinery and Electromechanics, University of Illinois. His research interests include all aspects of power electronic systems, with emphasis on nonlinear and large-signal analysis and control methods. He is the author of an undergraduate textbook *Elements of Power Electronics* (New York: Oxford University Press, 1998). He holds ten U.S. and European patents.

Dr. Krein received the 1990 IEEE Industry Applications Society First Prize Paper Award and the Fulbright Scholar Award, from 1997 to 1998, as a Visiting Reader at the University of Surrey, Guildford, U.K. He was President of the IEEE Power Electronics Society in 1999 and 2000. He was General Chair of the 1997 IEEE Power Electronics Specialists Conference. He is a registered Professional Engineer in the states of Illinois and Oregon.



**Richard M. Bass** (S'82–M'82–SM'94) was born in Jacksonville, FL, in 1959. He received the B.E.E. and M.S.E.E. degrees from the Georgia Institute of Technology (Georgia Tech), Atlanta, in 1982 and 1983, respectively, and the Ph.D. degree in electrical engineering from the University of Illinois, Urbana, in 1990.

From 1981 to 1983, he was employed by the Georgia Tech Office of Interdisciplinary Programs developing adaptive aids for persons with disabilities. From 1984 to 1987, he was employed by the Veterans Administration Rehabilitation R&D Unit, Atlanta, where he participated in the development of an improved motor drive for powered wheelchairs. He joined the faculty in the School of Electrical and Computer Engineering, Georgia Institute of Technology, in 1990 where he was an Associate Professor.